Interface effects in thermal conduction through molecular junctions: Numerical simulations

Yun Zhou and Dvira Segal[a)]
Department of Chemistry, Chemical Physics Theory Group, University of Toronto, 80 St. George Street, Toronto, Ontario M5S 3H6, Canada

(Received 29 May 2010; accepted 16 July 2010; published online 1 September 2010)

Thermal conductance in solid-molecule-solid junctions is studied within Langevin-type classical molecular dynamics simulations. The solids attached at the two ends, characterized by phonon bands mismatching the molecular vibrational window, are simulated using colored thermal noises with analytic correlation functions. We find that the dissimilarity in the vibrational spectra of the molecule and the interfacing materials crucially controls both the magnitude and the chain-length dependence of the heat current considering both harmonic and anharmonic molecules. By using reservoirs with distinct spectral functions, we also demonstrate that one can optimize the thermal rectifying (diodelike) properties of the junction. © *2010 American Institute of Physics*. [doi:10.1063/1.3475927]

I. INTRODUCTION

The process of heat conduction at the nanoscale naturally lends itself as a useful test bed for exploring fundamental topics in nonequilibrium thermodynamics and quantum mechanics: the role of many-body interactions in determining transport mechanisms,[1] the effect of the structure dimensionality,[2] and the relevance of quantum effects at the nanoscale.[3] Practically, controlling heat generation and thermal conduction in devices is a high-priority issue in electronics,[4] in particular, in molecular-level devices such as solid-molecule-solid junctions, self-assembled monolayers, and thin films.[5]

There are two types of thermal energy carriers in solids: electrons and phonons. While phonons dominate the thermal conduction properties of insulators and semiconductors, electrons predominantly control heat transfer in metals. However, considering metal-molecule-metal tunneling junctions with a poorly conducting molecule such as a hydrocarbon chain,[6] one can safely assume that since electron transmission is largely suppressed, only the structure vibrations are responsible for heat conduction.

Recent experiments on heat transfer in molecular junctions[6,7] and solid-molecule-liquid interfaces[8] have explored the underlying transport mechanisms and exposed the crucial role of the interface at the nanoscale. In these experiments the molecular chain, e.g., a hydrocarbon, typically includes $N \sim 5-10$ repeating units. Thus, unlike the mesoscopic limit, at the nanoscale the interface dramatically affects the dynamics.[9–13] Numerical simulations and theoretical studies have indeed manifested the influential role of the contacts (solids) on heat conduction in harmonic[14–16] and anharmonic lattices.[17,18] While these studies have typically focused on the asymptotic long-chain behavior, our objective here is to systematically study, through classical molecular dynamics (MD) simulations, the effect of the solids' spectral properties on thermal transport in *short to intermediate* size molecular junctions that are of experimental relevance. Specifically, it is of interest to simulate situations where there is a mismatch in the vibrational spectra of the attached solids and the molecule.[6,7] A schematic illustration of this setup is presented in Fig. 1. In what follows we refer to the solids attached to the molecular object as either thermal reservoirs, heat baths, or contacts.

Comprising the solid interface in a molecular dynamics simulation can be done either by explicitly including in the model Hamiltonian a few atomic layers of the substrate,[12] or by performing a Langevin-type dynamics, using the generalized Langevin equation (GLE).[19] Here, the spectral properties of the reservoirs are incorporated into frequency dependent damping terms, introducing memory effects, resulting in a non-Markovian dynamics.[20,21]

In a recent paper[22] we have followed the latter method, and investigated the heat conduction characteristics of molecular chains connected to non-Markovian (colored) reservoirs. However, only the simplified, easy to simulate, Ornstein–Uhlenbeck (OU) noise[23] has been employed: By introducing an auxiliary variable, the GLE with the OU noise can be simulated by a *Markovian* Langevin equation. Nevertheless, for simulating real solids with non-Ohmic phonon models, more flexible memory functions should be introduced, with (possibly) unknown Langevin-type dynamics.

In the present work we study the thermal conduction properties of molecular structures attached to non-Markovian reservoirs, by directly propagating the GLE, without reducing it to a Markovian Langevin equation. In particular, we numerically simulate the heat current through homogeneous chains of various sizes, characterizing the attached reservoirs by analytic phononic spectral functions with an adjustable spectral window. This enables us to analyze the role of the mismatch of the molecule-solids vibrational spectra on the junction thermal conductance and to consider resonance ef-

[a)]Electronic mail: dsegal@chem.utoronto.ca.

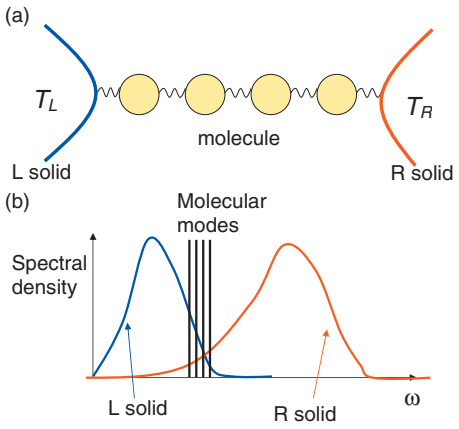

FIG. 1. (a) A schematic representation of our model, a 1D homogeneous molecular chain with two heat baths (solids) attached to its ends. (b) An illustration of the vibrational spectra of the interfacing solids and the interlocated molecule.

fects. Considering either harmonic or anharmonic internal molecular interactions, we find that the spectral properties of the reservoirs play a decisive role in determining the *length dependence* of the heat current. Thus, the thermal conductance of small nanojunctions should not be considered as a molecular property, rather its value reflects the hybrid object as a whole. By manipulating the dissimilarity in the vibrational spectra of the interfacing materials, introducing asymmetry, we also demonstrate that one can control the rectifying (diodelike) properties of anharmonic junctions.

This paper is organized as follows. Section II presents the model Hamiltonian and the equations of motion. Section III A describes the propagation scheme for a general time correlation function of the reservoirs fluctuations. In Sec. III B a simplified method for a specific, exponentially damped harmonic function is discussed. Section IV presented results considering solids with either similar or dissimilar vibrational spectra. Section V concludes.

II. MODEL

We consider a homogeneous molecule connecting two macroscopic solids, L and R, which are held at fixed temperatures T_L and T_R, respectively, $\Delta T=T_L-T_R$. In steady state there is a constant heat current between these two heat reservoirs through the molecule. A schematic representation of the model is depicted in Fig. 1. The Hamiltonian of this system is a sum of the molecular Hamiltonian, H_M, the Hamiltonian of the solid baths, H_n; $n=L,R$, and molecule-bath interaction terms, H_{ML} and H_{MR}. We model the molecule as a chain of one-dimensional (1D) N atoms, assuming a uniform system

$$H_M=\sum_{k=0}^{N}\left[\frac{p_k^2}{2m}+V(x_{k+1}-x_k)\right]. \tag{1}$$

x_k is the displacement from the equilibrium position of the kth particle of mass m and p_k is the particle momentum. The first ($k=0$) and the last ($k=N+1$) beads are the edge atoms of the contacts. A nearest-neighbors anharmonic force field is assumed for the interparticle potential energy V. The reservoirs are represented as collection of independent harmonic oscillators at thermal equilibrium

$$H_L=\sum_{l\in L}\left(\frac{1}{2}m_l\omega_l^2x_l^2+\frac{p_l^2}{2m_l}\right);\quad H_R=\sum_{r\in R}\left(\frac{1}{2}m_r\omega_r^2x_r^2+\frac{p_r^2}{2m_r}\right). \tag{2}$$

Only the end atoms of the molecular chain, $k=1,N$, are coupled to the solids, adopting a bilinear molecule-bath interactions[21]

$$H_{ML}=\sum_l\frac{1}{2}\frac{g_{1,l}^2x_1^2}{m_l\omega_l^2}-\sum_l g_{1,l}x_1x_l,,$$
$$H_{MR}=\sum_r\frac{1}{2}\frac{g_{N,r}^2x_N^2}{m_r\omega_r^2}-\sum_r g_{N,r}x_Nx_r. \tag{3}$$

The classical dynamics can be analytically represented in the form of a generalized Langevin equation[19]

$$\dot{x}_k=\frac{p_k}{m},\quad k=1,2,\ldots N,$$
$$\dot{p}_k=-\frac{\partial H_M}{\partial x_k},\quad k=2,3,\ldots,N-1,$$
$$\dot{p}_1=-\frac{\partial H_M}{\partial x_1}-\int_0^t dt'\,\gamma_L(t-t')p_1(t')+m\eta_L(t), \tag{4}$$
$$\dot{p}_N=-\frac{\partial H_M}{\partial x_N}-\int_0^t dt'\,\gamma_R(t-t')p_N(t')+m\eta_R(t),$$

where the effect of the thermal environments appears in Gaussian noise terms η_n; $(n=L,R)$ with zero mean, and damping terms (friction) $\gamma_n(t)$, satisfying the classical fluctuation-dissipation (FD) relation

$$\langle\eta_n\rangle=0;\quad\langle\eta_n(t)\eta_{n'}(t')\rangle=\frac{k_BT_n}{m}\gamma_n(|t-t'|)\delta_{n,n'}. \tag{5}$$

Here k_B is the Boltzmann constant, and the memory-damping kernel is, e.g., at the L end, $\gamma_L(t)=\frac{1}{m}\Sigma_l\frac{g_{1,l}^2}{m_l\omega_l^2}\cos(\omega_lt)$. It is related to the spectral function $J_L(\omega)=\frac{\pi}{2}\Sigma_l\frac{g_{1,l}^2}{m_l\omega_l}\delta(\omega-\omega_l)$ through

$$\gamma(t)=\frac{2}{m\pi}\int_0^\infty d\omega\frac{J(\omega)}{\omega}\cos(\omega t) \tag{6}$$

or in frequency domain, $J(\omega)=m\omega\gamma(\omega)$, where, $\gamma(\omega)=\int_0^\infty\gamma(t)\cos(\omega t)dt$. For the Ohmic (or Markovian) case, $\gamma(t)=2\gamma\delta(t)$ and $J(\omega)=m\gamma\omega$. Real environments are typically characterized by high frequency cutoff functions.

In what follows we consider a non-Ohmic form for the damping term $\gamma(t)$, and explain how we propagate the equations of motion (4) to yield the positions and velocities of all particles. The heat flux can be calculated from the trajectory using[24]

$$J = \frac{1}{2(N-1)} \sum_{k=1}^{N-1} \langle (v_k + v_{k+1}) F(x_{k+1} - x_k) \rangle, \tag{7}$$

where $F(r) = -\partial H_M(r)/\partial r$, $v_k = p_k/m$, and we average over time and ensemble after steady state is reached. We also calculate the junction thermal conductance K, defined as the ratio between the steady state heat current and the temperature difference

$$K \equiv J/\Delta T. \tag{8}$$

III. PROPAGATION SCHEME

A. Method

In order to study the dynamics under a general temporal correlation function $\gamma(t)$, the corresponding Gaussian process η has to be generated. For particular processes, e.g., the OU and Wiener (W) processes, the noise obeys a Langevin equation with a linear, Gaussian, white, noise term. Integration of this linear equation will generate the random processes with the particular time correlation. Such a method was followed in Ref. 22, simulating the conduction properties of molecular chains coupled to OU reservoirs. Here, in contrast, we are interested in Gaussian noises with a *general* temporal correlation function $\gamma(t)$, aiming in simulating realistic solids with certain phononic bands. In such cases a Markovian Langevin-like dynamics for the colored noise is not always known (or does not exist), and therefore, a more general algorithm that only depends on the knowledge of the temporal correlation should be adopted.[25–27] In such a scheme we first discretize the time into M intervals with a time step Δt, and construct a $2M \times 2M$ circulant matrix

$$A_{ij} = \begin{cases} \dfrac{k_B T_n}{m} \gamma_n(|t_i - t_j|) & \text{when } |i-j| < M \\ \dfrac{k_B T_n}{m} \gamma_n(|2(M-1)\Delta t - |t_i - t_j||) & \text{when } |i-j| \geq M, i,j = 1,2,\ldots,2(M-1). \end{cases} \tag{9}$$

The matrix A can be diagonalized by a discrete Fourier transform matrix F, $A = F\Lambda F^{\dagger}$, where Λ has positive entries for a well behaved function γ_n. It can be shown[25] that the real and the imaginary parts of $F\Lambda^{1/2}(x+iy)$ are both random vectors with the autocorrelation matrix A. Here x and y are random vectors with zero average and $\langle x_i x_j \rangle = \langle y_i y_j \rangle = \delta_{ij}$ correlations, Therefore, M sequential entries of x or y form a discrete realization of η_n. This random vector is then used to propagate Eq. (4) with a fourth-order Runge–Kutta method. The integral in Eq. (4) is calculated at each time step with the Simpson's rule, where in order to enhance performance, $\gamma_n(t)$ is truncated at time T at which $\gamma_n(T)$ is negligibly small. Matrix multiplications are carried out by the discrete Fourier transform subroutine library (FFTW3). Since A is a circulant matrix,[25] we only need to Fourier transform its first line to obtain the matrix Λ. The scheme is limited by the memory cost of storing the vector of noise realizations η_n.

B. Simplified equations for specific forms of $\gamma_n(t)$

The scheme described above is valid for general forms of $\gamma_n(t)$. However, the integral in Eq. (4) can be calculated more efficiently once rewritten in a differential form. For example, for an OU noise

$$\gamma_n^{(\mathrm{OU})}(t) = \frac{\epsilon_n}{\tau_n} \exp\left(-\frac{|t|}{\tau_n}\right),$$
$$\gamma_n^{(\mathrm{OU})}(\omega) \equiv \int_{-\infty}^{\infty} e^{-i\omega t} \gamma_n^{(\mathrm{OU})}(t) dt = \frac{2\epsilon_n}{1 + (\omega\tau_n)^2}, \tag{10}$$

of intensity ϵ and correlation time τ, we introduce two auxiliary dynamical variables

$$y_1(t) = \int_0^t dt' \gamma_L(t-t') p_1(t'),$$
$$y_N(t) = \int_0^t dt' \gamma_R(t-t') p_N(t') \tag{11}$$

satisfying the differential equations

$$\dot{y}_1 = \frac{\epsilon_L}{\tau_L} p_1 - \frac{1}{\tau_L} y_1,$$
$$\dot{y}_N = \frac{\epsilon_R}{\tau_R} p_N - \frac{1}{\tau_R} y_N. \tag{12}$$

Substitution of Eq. (11) into Eq. (4) results in a significant improvement of the numerical efficiency. Note that the OU noise can be alternatively simulated using a linear Langevin equation with a linear Gaussian white noise term.[22,28] However, in such a scheme, time integration error may cripple the

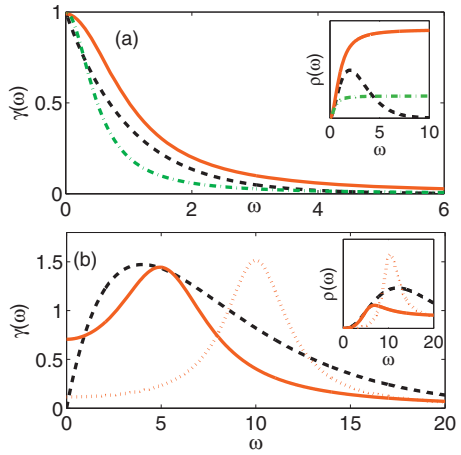

FIG. 2. Comparison between different forms for the damping function $\gamma(\omega)$. (a) A power law model [Eq. (16)] with $s=0$ and $\omega_c=1$ (dashed); A three-parameter model $\gamma^{(abc)}(\omega)$, see Eq. (14), with $a=1$, $b=0.1$, $c=0.5$ (full); The OU process, [Eq. (10)], with $\tau_c=2$, $\epsilon=0.5$ (dashed-dotted). The inset demonstrates the respective phonon density of states, $\rho(\omega)\propto\omega^2\gamma(\omega)$ for the three cases. (b) Power law model with $s=1$ and $\omega_c=4$ (dashed) and a three-parameter model $\gamma^{(abc)}(\omega)$ with $a=3$, $b=5$, $c=4$ (full) and $a=2$, $b=10$, $c=3$ (dotted). The inset demonstrates the respective phonon density of states.

FD relation (5). In contrast, in the present scheme, the colored noise is directly simulated using Eq. (9) to fulfill the FD relation at any time step.

The main physical drawback of the OU model is that it has a single controllable parameter τ determining the shape of the spectral density $J(\omega)$: Both the maximum position and the spectral width are controlled by $1/\tau$. To account for spectral functions of various shapes, and in particular to consider resonance effects, where the vibrational spectra of the molecule and the solids overlap, we introduce the more physically relevant exponentially damped harmonic form $(n=L,R)$ (Refs. 29 and 30)

$$\gamma_n^{(abc)}(t)=c_n\exp(-a_n|t|)\cos(b_n|t|) \tag{13}$$

with the Fourier transform

$$\gamma_n^{(abc)}(\omega)=\int_{-\infty}^{\infty}dt\exp(-i\omega t)c_n\exp(-a_n|t|)\cos(b_n|t|)$$

$$=\frac{2c_na_n(\omega^2+a_n^2+b_n^2)}{(a_n^2+\omega^2-2\omega b_n+b_n^2)(a_n^2+\omega^2+2\omega b_n+b_n^2)}. \tag{14}$$

Figure 2 illustrates the shape of this three-parameter (abc) damping function. It is peaked at

$$\omega_{\max}=[(a^2+b^2)^{1/2}\times(2b-\sqrt{a^2+b^2})]^{1/2} \tag{15}$$

with a maximum value of $\gamma^{(abc)}(\omega_{\max})=c\frac{a}{2b(\sqrt{a^2+b^2}-b)}$. The width is controlled by the parameters a and b. While this correlation function has been artificially constructed, it can serve as a useful tool for simulating the more realistic power-law model

$$\gamma^{(P)}(\omega)\propto\omega^s\exp(-\omega/\omega_c) \tag{16}$$

a widely accepted description of solids, where ω_c is the reservoir cutoff frequency and s is an integer. In Fig. 2 we illustrate the three spectral functions: $\gamma^{(\mathrm{OU})}(\omega)$, $\gamma^{(P)}(\omega)$ with $s=0,1$ and $\gamma^{(abc)}(\omega)$, demonstrating that the proposed structure [Eq. (14)] can reproduce some essential properties of a power law model: The onset of a maxima at a controllable frequency and a reduced density of states close to zero. This function is also useful for studying resonance effects as we can center it at a specific frequency [dotted line of Fig. 2(b)]. For clarity, we also include a schematic plot of the phonon density of states for each model, assuming $\rho(\omega)\propto\omega^2\gamma(\omega)$ [see discussion after Eq. (6)]. By tuning its parameters, the abc damping function can represent either an Ohmic bath, or a Debye-like spectrum. It should be also noted that while our molecular chain is strictly 1D, the baths' damping functions represent the phonon spectrum of a more realistic three-dimensional (3D) solid.[31]

Utilizing the form (14), the system dynamics can now be followed by defining two auxiliary dynamical variables, e.g., at the left contact

$$y_1(t)=c_L\int_0^t dt'\,e^{-a_L(t-t')}\cos[b_L(t-t')]p_1(t'),$$

$$z_1(t)=c_L\int_0^t dt'\,e^{-a_L(t-t')}\sin[b_L(t-t')]p_1(t') \tag{17}$$

satisfying the differential equations

$$\dot{y}_1=-a_Ly_1-b_Lz_1+c_Lp_1,$$

$$\dot{z}_1=-a_Lz_1+b_Ly_1. \tag{18}$$

Analogous equations hold at the right end

$$\dot{y}_N=-a_Ry_N-b_Rz_N+c_Rp_N,$$

$$\dot{z}_N=-a_Rz_N+b_Ry_N. \tag{19}$$

Substituting Eqs. (18) and (19) into Eq. (4) results in a stochastic differential equation without an integration term, which is more efficient to simulate.

IV. RESULTS

We describe first the molecular structure of the chain. We model the interactions between the atoms using a Morse potential of dissociation energy D, width parameter α, and an interatomic equilibrium separation x_{eq}

$$H_M=\sum_{k=1}^{N}\frac{p_k^2}{2m}+D\sum_{k=0}^{N}[e^{-\alpha(x_{k+1}-x_k-x_{eq})}-1]^2. \tag{20}$$

The atoms indexed by 0 and $N+1$ are the left and right reservoirs atoms. The following parameters are used: $D=3.84\times10^2/\nu^2$ kJ/mol, $\alpha=1.875\nu$ Å^{-1}, $x_{\mathrm{eq}}=1.54$ Å, and $m=12$ g/mol. Here ν is a parameter controlling the molecular anharmonicity, where for $\nu=1$ these numbers describe a c-c stretching mode.[32] We refer to the case of $\nu=0.01$ as the "harmonic model," yielding the characteristic molecular frequency $\omega_M=\sqrt{2D\alpha^2/m_r}\sim200$ ps^{-1}, where m_r is the reduced mass of the carbon atom.[33] The "anharmonic model," unless otherwise stated, refers to $\nu=6$. We have found (see repre-

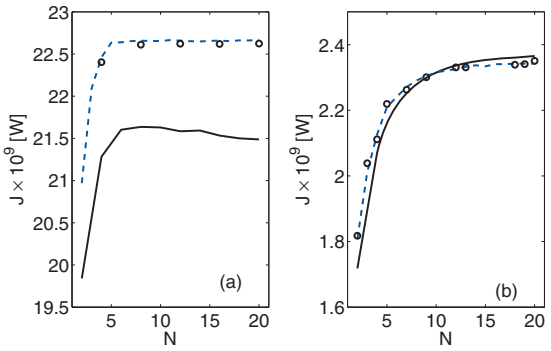

FIG. 3. Size dependence of the heat current in harmonic ($\nu=0.01$, dashed line) and anharmonic ($\nu=6$, full line) chains with non-Markovian heat baths. (a) OU noise with $\tau=0.01$ ps; (b) OU noise with $\tau=0.04$ ps. $T_L=300$ K, $T_R=0$ K, $\epsilon=50$ ps^{-1} in both cases. The circles were obtained using (the physical) $\nu=1$ model, essentially reproducing the harmonic results.

sentative results in Fig. 3) that the dynamics of a chain with the alkane force field ($\nu=1$) is well reproduced by the harmonic model $\nu=0.01$.[21] The Morse model with $\nu=6$ can be thought of as a hard-sphere potential with short range attractive interactions. We also present below [Fig. 10(c)] results for a Morse potential with $\nu=12$, representing a hard-sphere potential. To realize such a system experimentally one may either study the dynamics of hydrocarbons at very high temperatures, close to dissociation, or consider a colloidal suspension in a narrow constriction.

A. Symmetric junctions

We adopt first the OU spectral function, $\gamma_n^{(\mathrm{OU})}(t)=\frac{\epsilon_n}{\tau_n}e^{-|t|/\tau_n}$, and use the algorithm prescribed by Eqs. (11) and (12). In Fig. 3 we present the heat current for harmonic and anharmonic chains as a function of the molecular size N. Like the behavior discussed in Ref. 22, we find that if the reservoirs are characterized by a short memory time (Markovian limit) (i) harmonic junctions conduct better than anharmonic systems and (ii) the current in anharmonic systems decays with size. On the other hand, when the memory time of the reservoirs is long compared to the molecular time scale (inverse characteristic frequency), (i) the conductance

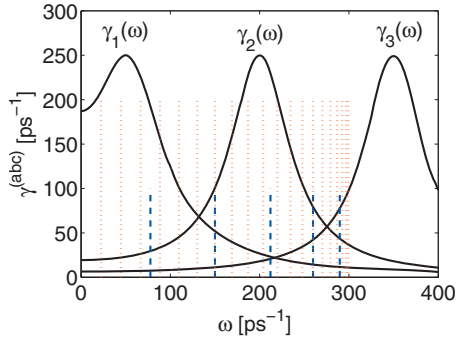

FIG. 4. Three abc damping functions [Eq. (14)], centered either below, $\gamma_1(\omega)$, in resonance, $\gamma_2(\omega)$, or above, $\gamma_3(\omega)$, the characteristic molecular frequency ω_M. The dashed (dotted) spikes are positioned at the normal mode frequencies of a 1D harmonic chain of length $N=5$ ($N=20$). The height of these vertical lines has no physical meaning here.

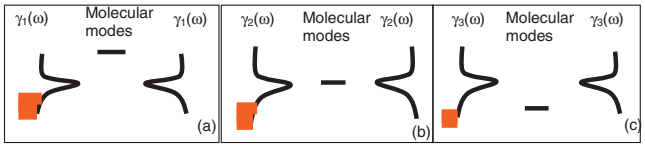

FIG. 5. Schematic representation of the three setups studied in Fig. 6. The shaded area at the left solid represents the populated bath modes. The solid line at the center stands for a characteristic molecular mode.

of anharmonic junctions increases with size and (ii) anharmonic junctions may conduct better than the corresponding harmonic junctions.[34]

In order to explore resonance effects, where the molecular vibrations overlap, or mismatch, with the solids' phonons, we simulate next the conduction properties of the molecular Hamiltonian (20) adopting the damping form (14), exposing the crucial role of the reservoirs' non-Markovian properties. We use three variants ($k=1,2,3$) of the *abc* spectral function, illustrated in Fig. 4, where in each case we assume that the reservoirs are identical, $\gamma_L^{(abc)}(\omega)=\gamma_R^{(abc)}(\omega)$. We define $\omega_{\max}$ as the frequency at which $\gamma^{(abc)}(\omega)$ is peaked. We further include the normal modes of a linear 1D chain of coupled harmonic oscillators of size $N=5$ (dashed spikes) and $N=20$ (dotted spikes), $\omega_n=\sqrt{2}\omega_M \sin[\pi n/2(N+1)]$; n is an integer, $1\le n\le N$. The three different setups considered are schematically depicted in Fig. 5.

Figure 6 demonstrates the length dependence of the current for each damping function. We find that depending on whether the reservoirs' spectral functions overlap with the molecular vibrations, centered around $\omega_M\sim 200$ ps^{-1}, or lay below or above them, the junction conductance significantly varies. In harmonic systems the current J_H saturates for long enough chains, $N>10$, irrespective of the reservoirs spectral properties, in agreement with the results of Ref. 21. In contrast, in anharmonic junctions the current J_A may either decrease, in (a) and (b), or increase (c) with size, delicately depending on the reservoirs properties: When the frequency window of the molecule and reservoirs overlap, $\omega_{\max}\sim\omega_M$, J_A weakly decays with length due to the increased importance of inelastic scattering processes, see Fig. 6(b). A log-log analysis further reveals that $J_A\sim N^{-0.1}$. Note that for $N=20$, $J_H/J_A\sim 1.5$, i.e., in the resonance case a harmonic junction better conducts than its anharmonic analog.

We turn to the case where the solids' phonon bands mismatch the molecular modes. In Fig. 6(a) we show the case

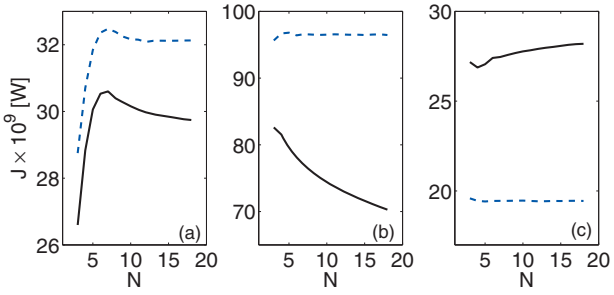

FIG. 6. Size dependence of the heat current in harmonic (dashed line) and anharmonic (full line) junctions. $T_L=300$ K, $T_R=0$ K. In (a)–(c), the left and right reservoirs' damping functions are $\gamma_k^{(abc)}(\omega)$ of Fig. 4, $k=1,2,3$, respectively.

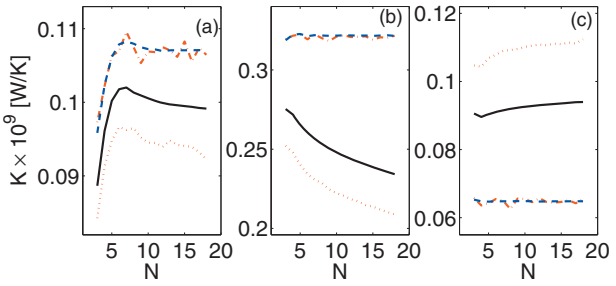

FIG. 7. Size dependence of the thermal conductance ($K=J/\Delta T$) in harmonic (dashed line) and anharmonic (full line) junctions for $T_L=300$ K, $T_R=0$ K; harmonic (dashed dotted line) and anharmonic (dotted line) junctions with $T_L=300$ K, $T_R=250$ K. All other parameters are the same as in Fig. 6.

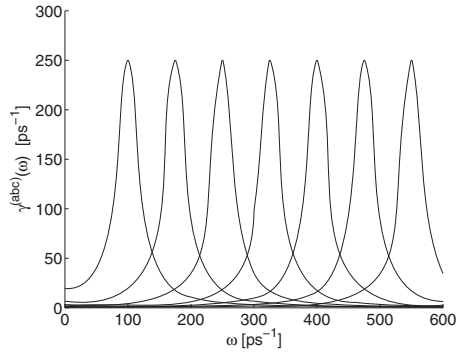

FIG. 8. A series of damping functions centered at $\omega_{\max}$, see Eq. (15), with a fixed maximum value $\gamma^{(abc)}(\omega_{\max})=250$ ps^{-1}.

$\omega_{\max}<\omega_M$, i.e., most (or all) molecular modes lay above the bath modes. Here both J_H and J_A first increase with size, then at a critical size, $N\sim 7$, J_H saturates, while J_A begins to decay. The fact that both J_H and J_A accordingly increase up to $N\sim 7$ hints that the underlying mechanism is common, probably the broadening of the molecular spectrum bringing it to resonance with the reservoirs modes. Figure 4 indeed supports this assertion. The normal modes of short chains are situated above the center of $\gamma_1(\omega)$: For $N=2$ the two molecular modes are located at $\omega_1\sim 150$ ps^{-1} and $\omega_2\sim 250$ ps^{-1} (not shown), while the modes of $N=5-7$ chain begin to overlap with $\omega_{\max}$. The vibrations of an $N=20$ chain already cover the relevant spectral window, $\omega_n=20-300$ ps^{-1}. Beyond the critical size $N=7$ transport is thus dominated by molecular modes in resonance with the bath phonon spectrum, and inelastic collisions become a significant factor, reducing J_A. In the oppositely detuned limit, $\omega_{\max}>\omega_M$, demonstrated in Fig. 6(c), we again observe a short-N dynamics in which J_H and J_A similarly behave. Beyond $N\sim 5$, J_H saturates, while J_A increases with size. This can be reasoned again as reflecting the increased importance of nonlinear interactions beyond a certain length, allowing for two-phonon recombination processes on the junction, leading to an enhancement of J_A in comparison to the harmonic component. Overall, quite significantly, in this case at $N=20$, $J_H/J_A\sim 0.6$.

In Fig. 7 we display the length dependence of the thermal conductance, $K\equiv J/\Delta T$, for two values of ΔT (50 and 300 K) for harmonic and anharmonic junctions. Note that the results at higher temperatures are more noisy, as a better averaging over time and the ensemble is necessary in order to achieve convergence. As expected, the harmonic results overlap at different temperature differences since $J_H\propto\Delta T$.[24] In contrast, the conductance of anharmonic systems depends on the actual junction temperature, where for higher $T_a=(T_L+T_R)/2$ the anharmonic and harmonic results more notably deviate. However, the qualitative length dependence of the (anharmonic) conductance stays intact irrespective of the temperature bias. We thus safely conclude that the results presented in Fig. 6 are representative for a broad range of temperatures.

We study next in details the effect of the bath spectral properties on the junction conductance. We generate a series of damping functions $\gamma^{(abc)}(\omega)$ (see Fig. 8). For each function, centered at $\omega_{\max}$, [see Eq. (15)], we calculate the heat current for a short chain of $N=5$ beads, considering either the harmonic limit with $\nu=0.01$ or the Morse interatomic potential with $\nu=6$. We again assume a symmetric junction with identical reservoirs, $\gamma_L^{(abc)}(\omega)=\gamma_R^{(abc)}(\omega)$. The results are presented in Fig. 9, manifesting the following features: If the baths' spectral functions overlap with the characteristic molecular frequency ($\omega_M\sim 200$ ps^{-1}) the harmonic system conducts better than its anharmonic counterpart. In contrast, when the molecular frequencies lay below the solids' band, $\omega_{\max}\gg\omega_M$, anharmonic junctions better conduct, as phonon-phonon scattering events contribute to energy transmission. In the opposite case, $\omega_{\max}<\omega_M$, harmonic junctions are more effective heat conductors, in agreement with the results of Fig. 6.

In Fig. 10 we demonstrate that this behavior is robust at various conditions: (a) at a smaller temperature difference, $\Delta T=50$ K, (b) for lower temperatures, and (c) assuming stronger anharmonicity, taking $\nu=12$ (modeling a hard sphere potential). We thus conclude that when the bulk characteristic frequencies exceed the molecular frequencies, anharmonic interactions lead to the enhancement of the heat current with respect to the harmonic value. This effect is marginal at low temperatures.

B. Junctions with solids of dissimilar spectra

Thermal flow asymmetry in two-terminal devices, displaying a greater heat flux in one direction than the other, has been experimentally observed in unevenly mass-loaded micron-scale nanotubes.[35] Generally, this thermal rectifying

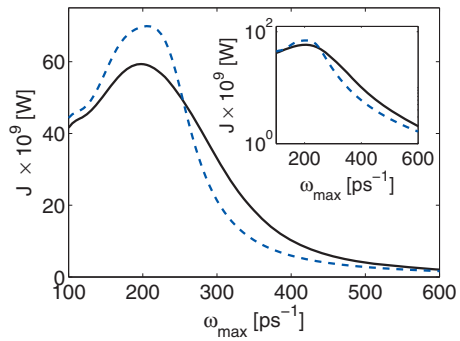

FIG. 9. Heat current as a function of $\omega_{\max}$, for a series of damping functions as illustrated in Fig. 8. Harmonic chain (dashed line); anharmonic chain (full line), $T_L=300$ K, $T_R=0$ K. The inset presents the data in a semilog scale.

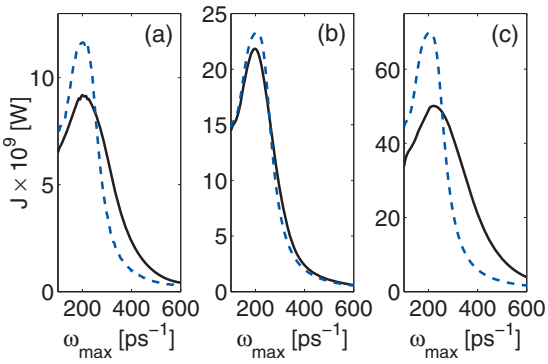

FIG. 10. Heat current as a function of ω_{max}, for a series of damping function as illustrated in Fig. 8. Harmonic chain (dashed line); anharmonic chain (full line). (a) $T_L=300$ K and $T_R=250$ K. (b) $T_L=100$ K and $T_R=0$ K. (c) $T_L=300$ K and $T_R=0$ K, assuming stronger interparticle anharmonic potential, $\nu=12$. All other parameters are the same as in Fig. 9.

effect is achieved when the device incorporates some spatial asymmetry combined with nonlinear (many-body) interactions.[36–39] It is of interest to understand the fundamental principles governing this effect,[40,41] and furthermore to control its direction[42] and enhance its magnitude.[43,44]

Here we combine reservoirs of dissimilar spectral properties, simulating distinct solids, e.g., a metal and a semiconductor, and calculate the heat current asymmetry in anharmonic chains. We find that the length dependence of the heat current is markedly distinct for forward and reversed operation modes, potentially leading to a significant rectification ratio for long chains. In particular, in Fig. 11 we employ dissimilar damping functions $\gamma_L^{(abs)}(\omega)$ with $\omega_{max}=50$ ps^{-1} and $\gamma_R^{(abs)}(\omega)$ with $\omega_{max}=250$ ps^{-1}, corresponding to the Debye frequencies of 8 and 40 THz, respectively. Recall that the molecular vibrations are centered around ~ 200 ps^{-1}. As expected, we find that harmonic chains do not rectify heat (data are overlapping), while in anharmonic systems the sign of the temperature bias does play a role: For $\Delta T<0$ ($T_L<T_R$) the current decays with size (□), while for $\Delta T>0$ it is enhanced with N. Overall, for $N\sim 20$, rectification ratio is $\mathcal{R}\equiv|J(\Delta T)/J(-\Delta T)|=1.1$.

The heat current is larger when flowing from a region

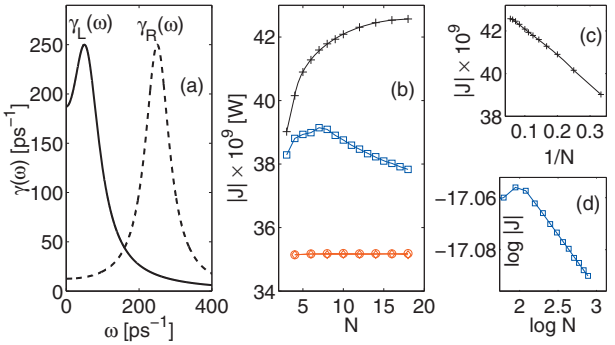

FIG. 11. Heat current in asymmetric junctions. (a) The reservoirs' spectral functions at the L side (full) and R side (dashed), $\gamma_L(\omega)\neq\gamma_R(\omega)$. (b) The magnitude of the heat current as a function of size for the harmonic force field (circle and diamonds overlapping) and the anharmonic force field with $T_L=300$ K and $T_R=0$ K(+); $T_L=0$ K, $T_R=300$ K (□). (c) and (d) analyze the anharmonic data of (b), wherein (c) the heat current $|J(\Delta T)|$ is plotted vs $1/N$. In (d) we show a log-log plot of $|J(-\Delta T)|$ vs size.

with a lower upper limit frequency (L reservoir) to a region with a higher upper limit frequency (R reservoir), in agreement with other studies.[40] When $T_L>T_R$, because of the existence of nonlinear effects, low frequency phonons from the L end inelastically scatter across the molecule to higher frequencies, thus they can transmit to the R end, accommodating only high frequency phonons. This effect is facilitated with increasing molecular size as more molecular modes overlap with the right bath. In the opposite limit of $T_R>T_L$, only very few R modes, at the tail of the spectrum, are populated, and inelastic effects should play their role twice: First, for transmitting thermal energy from the right side to the molecular modes, then for downconverting again the populated molecular modes to resonance with the low energy L phonons. Increasing the molecular size in this scenario actually decreases the current.

In Figs. 11(c) and 11(d) we further demonstrate the scaling laws of the heat current with chain size, for the anharmonic force field. For $\Delta T>0$ we obtain the qualitative behavior $J(\Delta T)=J_0-\beta/N$ with the asymptotic current value $J_0\sim 4.3\times 10^{-8}$ W and a slope $\beta\sim 13\times 10^{-9}$ W. For a negative bias, a log-log dynamics is obtained, $J(-\Delta T)\sim cN^{-\alpha}$, with $c\sim 4.3\times 10^{-8}$ W and the power $\alpha\sim 0.04$. Thus, for long chains the rectification ratio should slowly increase, $\mathcal{R}(N=30)\sim 1.2$.

It should be noted that the molecular anharmonicity employed in this study is enhanced, above the actual c-c force field value, in order to inflate the role of nonlinear interactions in molecular heat conduction. Generally, given a junction with some anharmonic interactions combined with structural asymmetry, we expect that rectification will be small for short chains, as harmonic interactions typically dominate at those sizes. Long chains, even of moderate anharmonicity, better rectifies. As asymmetry here is introduced at the boundaries, utilizing reservoirs with distinct properties, eventually for long enough (anharmonic) chains the contact effect will be marginal, and rectification will diminish. One could observe the rectification effect discussed here in realistic structures by adjoining two objects of distinct vibrational spectra, e.g., connecting metallic and semiconducting nanotubes. The chirality of such nanotubes is different, yet they can have an equal diameter, making the joint smooth.[45]

V. CONCLUSIONS

In this work we have studied the thermal conduction properties of solid-molecule-solid junctions using generalized Langevin equation simulations. The focus of this paper has been on the effect of the solids phononic spectral properties on the heat transport characteristics for harmonic and anharmonic molecules. Using an exponential-damped harmonic kernel, we mimicked the spectral density of solids with certain (high frequency or low frequency) phonon bands. It was found that the heat current characteristic is highly sensitive to the solid-molecule vibrational frequency mismatch. While for harmonic systems the current is constant for $N\gtrsim 5$, for anharmonic systems the current may either decay or increase with chain length, depending on the solid-molecule vibrational mismatch. We also found that

when the molecular vibrations are above the solids' characteristic frequency, harmonic junctions conduct better than their anharmonic counterparts, whereas in the opposite case nonlinear processes enhance the current beyond the harmonic value. Thus, while for molecules connected to Markovian (white noise) reservoirs anharmonic interactions generally lead to an increased resistance and reduction of current, in molecules coupled to colored reservoirs anharmonic effects may enhance the heat flux with chain length.

We have also demonstrated the effect of thermal rectification (thermal flow asymmetry) in anharmonic junctions made of interfacing materials with dissimilar vibrational spectra. Not only is the magnitude of the current distinct for forward and reversed biases, but the *current-length behavior* manifests a contrary dynamics, thus significant rectification ratio might be achieved for long chains. Specific realizations for our setup include, e.g., surfaces such as Pb and diamond. The dominant bands of the Pb vibrational spectra is in the 1–2 THz ($\omega_{\max} \sim 10$ ps^{-1} in our model) while for the diamond phonons lay in the range of 50–80 THz ($\omega_{\max} \sim 400$ ps^{-1}).[5] The molecular force field considered here relays on the 1D alkane chain parameters, with increased anharmonic parameters. In order to observe the nonlinear effects discussed here, one should consider molecules with strong nonlinear interactions.

It is of interest to further extend our study and consider a realistic 3D modeling of the nanoscale object: The current description of the alkane molecule admits only the stretching motion in the backbone. Allowing for the bending motion, including more degrees of freedom, should lead to the enhancement of the conductance, yet it is not clear whether the heat current *length dependence* would be significantly affected. Future study will be devoted to this issue. Quantum mechanical effects were completely dismissed in this work and a purely classical treatment has been adopted here. A simple route for incorporating some quantum effects into a Langevin-type treatment would involve replacing the classical reservoirs (solids) by quantum heat baths accounting for quantum statistics.[46,47]

Besides the fundamental interest in the transport mechanism of nonlinear microscopic systems, manipulating flow of thermal current at the nanoscale might be useful in applications: for increasing the efficiency of thermoelectric devices,[48] for constructing phonon filters improving thermal insulation,[5] and for realizing active thermal devices, e.g., (single-molecule) phonon transistors,[49] thermal logic gates,[50] or memory elements.[51]

ACKNOWLEDGMENTS

This research has been supported by a grant from the Natural Sciences and Engineering Research Council of Canada. Computations were performed on the GPC supercomputer at the SciNet HPC Consortium. SciNet is funded by the Canada Foundation for Innovation under the auspices of Compute Canada, the Government of Ontario, Ontario Research Fund-Research Excellence, and the University of Toronto.

[1] A. Dhar, Adv. Phys. **57**, 457 (2008).
[2] K. Saito and A. Dhar, Phys. Rev. Lett. **104**, 040601 (2010).
[3] J.-S. Wang, J. Wang, and J. T. Lü, Eur. Phys. J. B **62**, 381 (2008).
[4] E. Pop, Nano Res. **3**, 147 (2010).
[5] V. P. Carey, G. Chen, C. Grigoropoulos, M. Kaviany, and A. Majumdar, Nanoscale and Microscale Thermophys. Eng. **12**, 1 (2008) and references therein.
[6] R. Y. Wang, R. A. Segalman, and A. Majumdar, Appl. Phys. Lett. **89**, 173113 (2006).
[7] Z. Wang, J. A. Carter, A. Lagutchev, Y. K. Koh, N.-H. Seong, D. G. Cahill, and D. D. Dlott, Science **317**, 787 (2007); J. A. Carter, Z. Wang, H. Fujiwara, and D. D. Dlott, J. Phys. Chem. A **113**, 12105 (2009).
[8] Z. Ge, D. G. Cahill, and P. V. Braun, Phys. Rev. Lett. **96**, 186101 (2006).
[9] H. A. Patel, S. Garde, and P. Keblinski, Nano Lett. **5**, 2225 (2005).
[10] X.-P. Zhang and J.-D. Bao, Phys. Rev. E **73**, 061103 (2006).
[11] G. Kikugawa, T. Ohara, T. Kawaguchi, E. Torigoe, Y. Hagiwara, and Y. Matsumoto, J. Chem. Phys. **130**, 074706 (2009).
[12] T. Luo and J. R. Lioyd, ASME J. Heat Transfer **132**, 032401 (2010); Int. J. Heat Mass Transfer **53**, 1 (2010).
[13] L. Nicolin and D. Segal, Phys. Rev. E **81**, 040102 (2010).
[14] K. Saito, S. Takesue, and S. Miyashita, Phys. Rev. E **61**, 2397 (2000).
[15] A. Dhar, Phys. Rev. Lett. **86**, 5882 (2001).
[16] L. W. Lee and A. Dhar, Phys. Rev. Lett. **95**, 094302 (2005).
[17] H. Zhao, L. Yi, F. Liu, and B. Xu, Eur. Phys. J. B **54**, 185 (2006).
[18] D. Barik, Eur. Phys. J. B **56**, 229 (2007).
[19] U. Weiss, *Quantum Dissipative Systems* (World Scientific, Singapore, 1999).
[20] P. Hänggi, Lect. Notes Phys. **484**, 15 (1997).
[21] D. Segal, A. Nitzan, and P. Hänggi, J. Chem. Phys. **119**, 6840 (2003).
[22] D. Segal, J. Chem. Phys. **128**, 224710 (2008).
[23] G. E. Uhlenbeck and L. S. Ornstein, Phys. Rev. **36**, 823 (1930).
[24] S. Lepri, R. Livi, and A. Politi, Phys. Rep. **377**, 1 (2003).
[25] A. T. A. Wood and G. Chan, J. Comput. Graph. Stat. **3**, 409 (1994).
[26] J. García-Ojalvo, J. M. Sancho, and L. Ramirez-Piscina, Phys. Rev. A **46**, 4670 (1992).
[27] K. Lü and J.-D. Bao, Phys. Rev. E **72**, 067701 (2005).
[28] J. Łuczka, Chaos **15**, 026107 (2005).
[29] L. Schimansky-Geier and C. Zülicke, Z. Phys. B: Condens. Matter **79**, 451 (1990).
[30] R. L. S. Farias, R. O. Ramos, and L. A. da Silva, Phys. Rev. E **80**, 031143 (2009).
[31] N. W. Ashcroft and N. D. Mermin, *Solid State Physics* (Saunders, Philadelphia, 1976).
[32] S. Lifson and P. S. Stern, J. Chem. Phys. **77**, 4542 (1982).
[33] For a 1D monoatomic harmonic chain of size N, connected to two solids at both ends, the normal modes frequencies are given by $\omega_n = 2\sqrt{K/m}|\sin[n\pi/(N+1)]$; $1 \le n \le N$. Here K is the spring constant and m is the atomic mass. In terms of the Morse parameters, expanding the Morse potential near equilibrium [Eq. (20)] we find $K = 2D\alpha^2$. For the alkane chain the highest vibrational frequency is thus $\sqrt{2}\sqrt{2D\alpha^2/m_r} \sim 300$ cm^{-1} ; m_r is the reduced mass. As a measure for the characteristic molecular frequency we define $\omega_M = \sqrt{2D\alpha^2/m_r} \sim 200$ cm^{-1}, lying inside the molecular spectrum.
[34] In comparing the results presented in Fig. 3 and Ref. 22 note that the force field parameters were slightly modified. This leads to a small modification in the current characteristics at a given memory time τ.
[35] C. W. Chang, D. Okawa, A. Majumdar, and A. Zettl, Science **314**, 1121 (2006).
[36] M. Terraneo, M. Peyrard, and G. Casati, Phys. Rev. Lett. **88**, 094302 (2002).
[37] B. Li, L. Wang, and G. Casati, Phys. Rev. Lett. **93**, 184301 (2004); B. Li, J. H. Lan, and L. Wang, *ibid.* **95**, 104302 (2005).
[38] D. Segal and A. Nitzan, Phys. Rev. Lett. **94**, 034301 (2005); J. Chem. Phys. **122**, 194704 (2005).
[39] J. Lan and B. Li, Phys. Rev. B **74**, 214305 (2006); J. H. Lan and B. Li, *ibid.* **75**, 214302 (2007); N. Yang, N. Li, L. Wang, and B. Li, *ibid.* **76**, 020301 (2007).
[40] N. Zeng and J.-S. Wang, Phys. Rev. B **78**, 024305 (2008).
[41] L.-A. Wu and D. Segal, Phys. Rev. Lett. **102**, 095503 (2009); L.-A. Wu, C. X. Yu, and D. Segal, Phys. Rev. E **80**, 041103 (2009).
[42] L.-F. Zhang, Y.-H. Yan, C.-Q. Wu, J.-S. Wang, and B. Li, Phys. Rev. B **80**, 172301 (2009).
[43] G. Casati, Nat. Nanotechnol. **2**, 23 (2007).
[44] N. Yang, G. Zhang, and B. Li, Appl. Phys. Lett. **93**, 243111 (2008).

[45] J.-C. Charlier, X. Blase, and S. Roche, Rev. Mod. Phys. **79**, 677 (2007).
[46] J.-S. Wang, Phys. Rev. Lett. **99**, 160601 (2007).
[47] H. Dammak, Y. Chalopin, M. Laroche, M. Hayoun, and J.-J. Greffet, Phys. Rev. Lett. **103**, 190601 (2009).
[48] A. I. Hochbaum, R. K. Chen, R. D. Delgado, W. J. Liang, E. C. Garnett, M. Najarian, A. Majumdar, and P. D. Yang, Nature (London) **451**, 163 (2008).
[49] B. Li, L. Wang, and G. Casati, Appl. Phys. Lett. **88**, 143501 (2006); M. G. Menezes, A. Saraiva-Souza, J. Del Nero, and R. B. Capaz, Phys. Rev. B **81**, 012302 (2010).
[50] L. Wang and B. Li, Phys. Rev. Lett. **99**, 177208 (2007).
[51] L. Wang and B. Li, Phys. Rev. Lett. **101**, 267203 (2008).